Applied Catalysis B: Environmental 304 (2022) 120946

Contents lists available at ScienceDirect

Applied Catalysis B: Environmental

journal homepage: www.elsevier.com/locate/apcatb

Visible light-driven carbon-carbon reductive coupling of aromatic ketones activated by Ni-doped CdS quantum dots: An insight into the mechanism

Rong Hu [a,1], Wei-Hua Xie [a,1], Hong-Yan Wang [a,*], Xin-Ai Guo [a], Hua-Ming Sun [a], Cheng-Bo Li [c], Xue-Peng Zhang [b,*], Rui Cao [b,*]

[a] Key Laboratory for macromolecular Science of Shaanxi Province, School of Chemistry and Chemical Engineering, Shaanxi Normal University, Xi'an 710119, PR China
[b] Key Laboratory of Applied Surface and Colloid Chemistry, Ministry of Education, School of Chemistry and Chemical Engineering, Shaanxi Normal University, Xi'an 710119, PR China
[c] College of Chemistry & Materials Science, Northwest University, Xi'an 710127, PR China

ARTICLE INFO

Keywords:
Selectively reductive coupling
Carbon-carbon bond formation
Ketone activation
Visible-light catalysis
Proton-coupled electron transfer

ABSTRACT

Photocatalytic reductive coupling of carbon-carbon bond to assemble complex molecular frameworks holds the great promising for solar energy storage and value-added chemicals production. This process generally demands noble-photosensitizer or powered by ultraviolet light, along with harsh conditions, which inevitably induces undesired by-product with poor selectivity. Here, we demonstrated selectively reductive aromatic ketones into pinacol on low-cost photocatalysts Ni-doped quantum dots, in which the yield can reach up to 88% with ketones conversion more than 95% under visible-light irradiation for 5 h. A novel mechanism dedicated to the interaction between in situ generated oxidized sacrificial agents $TEA^{\bullet+}$ and reactants for key ketyl radical formation via proton-coupled electron transfer (PCET) is elaborately probed by EPR measurement, iotope labeling experiments and DFT calculation. This work emerges a new family of catalysts for C-C coupling by solar energy. More importantly, it provides more credible demonstration for TEA activated photocatalytic conversion in organic synthesis.

1. Introduction

The blossom of atom-economic and step-efficient carbon-carbon bond to assemble complex molecular frameworks has witnesse`d its considerable importance in organic synthesis over the century [1]. As one of the most efficient reactions to create C-C bonds, the synthesis of pinacol has long been attracted intense attentions. This is because pinacol emerges as common structural intermediates in pharmaceuticals and agrochemicals, and they are also of vital importance as structural motifs in natural products [1a,2]. For general synthesis, one of the most promising protocols dedicated to direct reductive dimerization of readily available carbonyl moiety via pinacol-coupling reaction. In the aid of low-valent metals Cu, Zn and Mg, the reaction entails via single-electron-transfer (SET) process from metal to carbon groups for affording the corresponding ketyl radical intermediates, which undergo coupling to form C-C bond [3]. Unfortunately, due to high activation-energy barriers, such classical protocol usually requires more than stoichiometric amount of metal catalyst loading, which also poses severe issues with air sensitivity, functional-group tolerance, unwanted side reaction, and a large quantity of unavoidable waste products.

As an abundant and renewable energy resource, light, particularly visible-light, enables to provide driving force for chemical reactions [4]. Some light-harvest semiconductors with suitable band levels can absorb sunlight and create separated electrons and holes for participating into typical redox reactions. Recent interests in visible-light mediated oxidation of alcohols become an effective pathway to evolve pinacol [5]. In comparison, reduction of carbonyl is much more attractive, largely because the most biomass-derived molecules are naturally C═O rich, and also because catalytic reduction can incorporate pinacol synthesis into biomass transformation. More importantly, reduction of C═O can endow the conversion with advantages to construct potential chiral centers, which will push reduction catalysis to achieve further improvements. Nevertheless, so as to deliver carbon radical for C-C bond coupling, photo-induced pinacol production usually demands high-energy ultraviolet light irradiation to activate C═O [7]. Molecular photosensitizers have been recognized as a powerful tool for the

* Corresponding authors.
E-mail addresses: hongyan-wang@snnu.edu.cn (H.-Y. Wang), zhangxp@snnu.edu.cn (X.-P. Zhang), ruicao@snnu.edu.cn (R. Cao).
[1] The authors contributed equally.

https://doi.org/10.1016/j.apcatb.2021.120946
Received 19 September 2021; Received in revised form 15 November 2021; Accepted 16 November 2021
Available online 25 November 2021

synthesis of pinacol, in which the photocatalytic generation of ketyl radicals from carbonyls following a proton-coupled electron transfer (PCET) process is recently reported by Knowles [6]. However, those homogeneous photocatalytic approaches demand noble metals molecular photosensitizers containing Ir or Ru and so forth. Besides, the requirement of strong alkaline with long reaction time (usually more than 15 h) inevitably induce undesired by-product with poor selectivity [1a,7]. Very recently, two-dimensional $ZnIn_2S_4$ nano-sheets were employed by Sun to achieve photocatalytic benzaldehyde transformation into hydrobenzoin upon visible-light irradiation in the presence of a sacrificial electron donor [8]. Although high conversion efficiency of the reagent highlights the promising of this approach in practical applications, its activation was restricted to few specific aldehydes and its use for the activation of ketones has been poorly developed [3a,9].

Among the numerous pioneering semiconductors, CdS quantum dots (QDs) are attractive to function as ideal light absorbers and photocatalysts in the application of light-driven water splitting and CO_2 reduction [10]. CdS QDs can trigger out massive redox equivalents (excited electrons and holes) for the sequent charge replenishments, thus it is typically essential for photoredox catalysis of organic reactions [11]. In order to effectively deactivate the photogenerated charge for surface reaction and protect QDs from severe light corrosion, we recently proved that binding multiple surfactants on the surface of CdS QDs can significantly improve photo-reductive activity and stability [10d]. Hence, we supposed that it might be a feasible strategy to extend CdS QDs photocatalysts for visible-light-driven selective reduction of ketones into pinacol. Although the very recent works for C-C coupling on CdS quantum dots have been reported by McClelland and Weiss [5a] or Wu [5c] respectively, those works focus on how to oxidize alcohol into pinacol. Much more differently, a mixture of hydrobenzoin, deoxybenzoin, and benzil were obtained, leading to poor selectivity for C-C formation [5]. Here, we report an efficient and durable system for reductive coupling of aromatic ketones into pinacol based on Ni^{2+}-doped CdS QDs (Ni&CdS QDs) under visible-light irradiation with desirable selectivity using TEA as sacrificial agent. Implanting Ni dopants is evidenced to enhance the electron trapping in sulfur vacancies, along with substantially promoted charge separation on CdS surface [12]. Mechanism studies validated TEA feathered to activate reactant, which renders a PCET process to umpolung ketone into key ketyl radical [3a, 6]. To the best of our knowledge, this is the first explicit demonstration on the base metal incorporated semiconductors for photocatalytic reductive coupling of aromatic ketones for pinacol generation under visible-light irradiation. Moreover, the overall mechanistic pathway lays the foundation to validly understand substrate-activated function of sacrificial TEA and high-selectivity over a light motivated system.

2. Experimental section

2.1. Materials

All reactions were carried out under an atmosphere of nitrogen, unless otherwise specified. After further purification, CH_3CN and Triethylamine were used. Without special stated, the chemicals were purchased from Energy Chemical Co., Ltd, while DMPO (dimethyl pyridine N-oxide) used for EPR was obtianed from Dongren Chemical Technology Co., Ltd. For purification of crude reaction product, thin layer chromatography (TLC) with 300–400 mesh silica gel was applied.

2.2. Characterization

UV-Vis diffuse reflectance spectra (UV-Vis DRS) were operated on UV-Vis-NIR spectrometer (Perkin-Elmer, USA) at room temperature from 300 to 800 nm with $BaSO_4$ as background. High resolution mass spectrometry (HR-MS) was measured on German Bruker MAXIS. NMR data (^1H NMR and ^{13}C NMR) was recorded with 400 MHz Bruker, in which Chemical shift is expressed in parts per million (ppm) unit with TMS as standard. Inductively coupled plasma mass spectrometry (ICP-MS) for the element content was determined after the sample was dissolved in chromatographically pure concentrated nitric acid, which was then diluted with 1% nitric acid into the range of 100–400 ppm. German Bruker EMX-10/12 electronic paramagnetic spectrometer was applied to collect Electron paramagnetic resonance spectroscopy (EPR) data to detect the generation of free radicals in illumination system. Hydrogen detection and quantification was carried out through TCD detection port on Tianmei GC7900 gas chromatograph, with CH_4 as internal standard. Liquid product was detected on Agilent GC7860A gas chromatograph with the extracted sample vaporized on the instrument with the retention time of pure standard complex as standard, which was quantified based on calibration curve of pure standard complex.

2.3. The preparation of 0.20% Ni&CdS QDs catalyst

Under nitrogen atmosphere, $CdCl_2{\cdot}2H_2O$ (114.2 mg, 0.57 mmol) was dissolved into 100 mL H_2O, in which an aqueous solution of $NiCl_2$ (150 μL, 0.01 M) was added. Then 3-mercaptopropionic acid (MPA) (500 μL, 11.5 mmol) was injected, and the pH was adjusted to 7 with 1 M NaOH. During the reaction, the colorless solution changed into white turbid liquid and eventually a colorless transparent solution was obtained. After 5 mL of 0.1 M Na_2S solution was added and refluxed at 100 °C for 4 h, it delivered a clear bright yellow solution, which was then evaporated to remove excess water and afforded a yellow viscous liquid. A large amount of isopropanol was added to precipitate the system, then the product was centrifuge. After repeating the above operation for twice, the photocatalyst was obtained as a yellow solid 43 mg. For the synthesis of CdS QDs doped with other content of nickel, the same operation was applied with corresponding concentration of $NiCl_2$ solution instead.

2.4. The preparation of photocatalytic system

The photocatalytic reduction of carbonyl compounds was carried out in a quartz test tube (15 mL) under constant magnetic stirring at room temperature, in which the top was sealed by a high-quality septum. In a typical experiment, 10 mg photocatalyst was dissolved in the mixture with 3 mL water and 1 mL CH_3CN, then 1 mL TEA was added as the sacrificial agent, and finally the substrate acetophenone (234 μL, 0.4 M, 2 mmol) was injected. After being purged with N_2 for 30 min, the system was sealed and reacted under irradiation with $\lambda = 420$ nm LED (the input optical power is 8.37 mW cm^{-2}) for a certain time.

2.5. Computational Methodology

Density functional theory (DFT) calculations were carried out using the Gaussian 16 program package [13]. Geometry optimizations and harmonic frequency calculations were conducted at the level of D3(BJ) [14]-B3LYP [15]/Def2-SVP [16]. Single point energy refinements were conducted on the optimized structures at the level of D3 (BJ)-B3LYP/Def2-TZVP. The solvation effects in aqueous solution were estimated by utilizing polarized continuum model (PCM) [17] with the SMD [18] atomic radii. For redox potential calculations, reference potential of standard hydrogen electrode (SHE) was set as − 4.28 V [19]. The atomic charges conducted by natural population analysis (NPA) [20] were utilized. All thermodynamic data were reported in 298.15 K and 1 atm.

3. Results and discussion

3.1. Photocatalytic C-C reductive coupling of ketones

3.1.1. Photocatalytic C-C reductive coupling of acetophenone

Photocatalyst Ni^{2+}-doped CdS QDs was reported by Xiong for

selective CO_2 reduction under visible-light irradiation [12d], which was obtained by us with appropriate modification (see SM). With TEA as the sacrificial agent, the reductive coupling of acetophenone to deliver pinacol was initially chosen as a model reaction. Prior to irradiation, the system was saturated by N_2 to remove O_2. The product was purified after column chromatography, which was further well characterized by ^1H NMR, ^{13}C NMR and mass spectrometry (MS). On the basis of calibration curves, the amount of generated pinacol was quantified by gas chromatography (GC). Control experiment indicates that no pinacol was produced under darkness. Contrarily, irradiation can boost the conversion of acetophenone. Fig. 1 plots the yield profile of pinacol produced from acetophenone versus the irradiation time over Ni&CdS with a loading of 0.20% Ni^{2+} on QDs under a 420 nm LED irradiation. It is found that the amount of pinacol increased with the irradiation time at the first 5 h. Prolonging the irradiation time could not further polish up the efficiency, but the color of the QDs colloidal changed gently from the original bright yellow to dark gray during the photocatalytic reaction. However, when irradiation was switched off, the reaction system turned to initial yellow upon standing for couple of hours. Such phenomenon was also observed in a CdS and Ru-hybrid mixed system for photocatalytic hydrogenation reaction by Li et al. [4b]. Based on their analysis, the color change of QDs colloidal into dark gray is attributed to the partial oxidation of S^{2-} into polysulfide ions (S_x^{2-}) in CdS matrix by valence holes [4b,12c], and the color recovery implies that polysulfide ions (S_x^{2-}) can be reversibly reduced back to S^{2-} under darkness in the presence of sacrificial donor [4b,12b]. Considered the consumption of TEA after the first 5 h, the reaction system after irradiation was preserved under the dark for 2 h, together with replenishment of TEA, which can bring out a sustained progress in reaction as expected, affording pinacol yield up to 73%. This observation suggests that although the decomposition of CdS was inevitable, the activity for photocatalysis can be expectedly brought back by both recovery of CdS and supplement of sacrificial agent. We further validated the reproducibility of the reaction and also carried out control experiments, which proved that light, sacrificial agent, photocatalyst are all required for photocatalytic pinacol production.

Usually, pH can seriously interfere with the outcome of photocatalytic reaction. Therefore, pH dependence results were further carefully investigated, depicted as Fig. S1. It is found that the delivered yield of pinacol improved by increasing pH (higher than 10), but it was seriously restricted in acidic or neutral conditions [21]. Besides of pinacol, alcohol was observed as another reductive liquid product, albeit with much lower yield. Simultaneously, H_2 was also detected in the headspace of reaction vials. Careful quantification provides the distinct evidence that the appearance of acetophenone substrate inhibited H_2 evolution; and the higher substrate concentration the higher inhibition (Fig. 2). It implies that hydrogen evolution and pinacol production both resulted from the reduction reaction, where electron generated from excited photocatalyst after irradiation can react with water to liberate hydrogen, and also can be captured by acetophenone for the generation of pinacol. Therefore, the fact that H_2 evolution was suppressed in the presence of acetophenone highlights a competing pathway for H_2 production and acetophenone reduction.

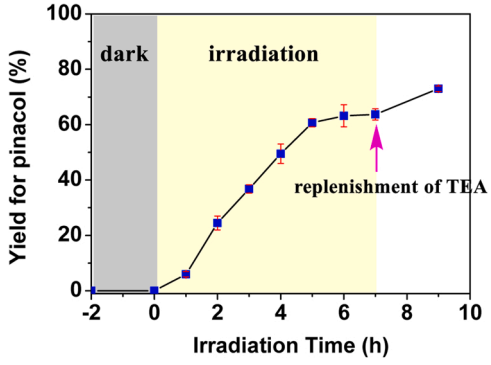

Fig. 1. Yield of pinacol as a function of irradiation time in a total 5 mL reaction system (H_2O: CH_3CN: TEA = 3:1:1) with 0.20% Ni&CdS (10 mg), and acetophenone (2 mmol) under irradiation of LED (λ = 420 nm, the input optical power is 8.37 mW cm^{-2}). The arrow indicates the time when the irradiated system was kept in dark after 2 h and the replenishment of TEA (0.5 mL) was carried out.

3.1.2. *Effect of dopant concentration on photocatalytic performance*

To shed light on the effect of dopant concentration on photocatalytic performance, a series of Ni&CdS QDs with different Ni contents was prepared. As shown in Table S1, photocatalytic activity followed a trend with the maximum activity observed at 0.20% Ni contents. Characterization of materials indicates that Ni&CdS QDs with 0.20% Ni (0.20% Ni&CdS) shows the widest absorption edge in the visible-light region (Fig. S2). Since the optical absorption in the wavelength region is originated from free-carrier absorption of conduction electrons, it marks that 0.20% Ni&CdS holds the greatest carrier concentration, agreeing on the best visible-light driven photocatalytic activity [22a]. Typically, the conversion of acetophenone over 0.20% Ni&CdS approached to 94%, accompanied by producing pinacol with a 63% yield after 5 h irradiation, while the competing reduction to 1-phenylethanol was virtually prevented. Note that only 16% yield of pinacol is generated by pristine CdS QDs, much lower than the impressive value obtained over Ni&CdS QDs, which implies that Ni dopants imposed the significant influence on ketone reduction. Photocatalyst 0.20% Ni&CdS was characterized by XPS (X-ray Photoelectron Spectroscopy) (Fig. S3). There is no signal ascribed to Ni in XPS due to its much lower loading content. However, based on ICP-MS (Inductively Coupled Plasma Mass Spectrometry), Ni can be well determined with the content as 0.55 μg/mg in 0.20% Ni&CdS.

Standard catalytic condition: 0.20% Ni&CdS (10 mg), Substrate (2 mmol), TEA (1 mL), CH_3CN (1 mL), H_2O (3 mL), irradiated by LED (λ = 420 nm, the input optical power is 8.37 mW cm^{-2}) for 5 h under N_2 at room temperature. Yield after work up (average of at least three parallel tests) determined by GC analysis relative to calibrated internal standard. Addition of CH_3CN is in order to maintain the reasonable solubility of substrates in photocatalytic solution.

3.1.3. *Reaction scope based on different substrate*

Under the optimized reaction conditions, the scope and limitations of this protocol were investigated. The reaction scope was tested with 0.20% Ni&CdS QDs. A wide range of alkyl aryl ketones can be reduced to corresponding pinacol in a H_2O: CH_3CN: TEA (v: v: v = 3: 1: 1, mL) aqueous solution under N_2 with irradiation for 5 h, which was summarized in Table 1. In general, isolated yields and selectivity are acceptable, but the results are affected by the size of alkyl group on ketone as well as the electronic effect of substitution. The small substituent at para-position of benzene ring (subs. 1–2) resulted in an ideal conversion of parent ketone to final C-C coupling products. Conjugated group combined with aromatic groups can fascinate a nearly quantitative conversion to corresponding pinacols. The electronic effects of substrate influence the reaction. Electron-rich ketones gave lower pinacol yields such as subs. 4 (22%), but relatively higher conversion obtained with electron-withdrawing substituent (subs. 5, 53%), which is in line with the fact that electron-withdrawing groups render the C═O group easier to be reduced. The methodology tolerates the ketone with different group on alkyl part (subs. 6–10), but the products varied with the size and electronic function of the groups. H and alkyl groups were compatible in the transformation, albeit giving slightly lower yields (25–42%). Aromatic group can suppress the formation of pinacol, which generates the corresponding reduced alcohol product instead (subs. 7). As expected, bulk groups restrict the generation of organic products, where neither pinacol nor alcohol was investigated, but only a large amount of H_2 was observed (subs. 8). This result is in accordance with

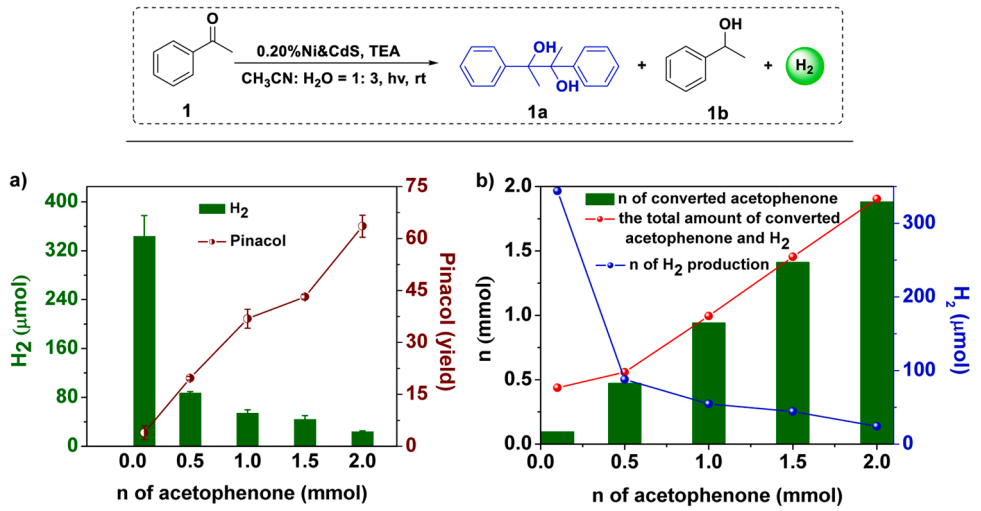

Fig. 2. a) the photo-generated H_2 and pinacol with the concentration of acetophenone; b) the total amount of photo-generated H_2 and converted acetophenone with the concentration of acetophenone over 0.20% Ni&CdS photocatalyst for 5 h.

Table 1
Photocatalytic reduction of selected aromatic ketones and aldehy.

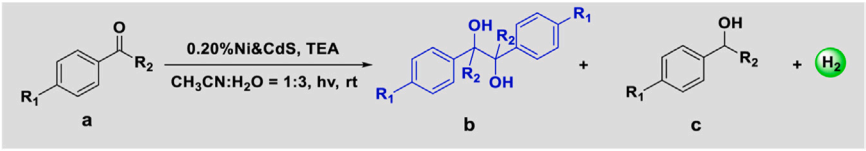

Entry	-R1	-R2	Liquid products yield (%)		Conversion of substrate (%)	Gas products (μmol)
			Alcohol	Pinacol		H_2
1	H	Me	<2	63	94	24
2	Me	Me	<1	88	95	49
3	Ph	Me	4	85	93	50
4	OMe	Me	<1	22	80	37
5	CF_3	Me	0	53	96	38
6	H	n-propyl	0	42	72	51
7	H	Ph	65	0	94	28
8	H	CPh_3	0	0	0	374
9	H	H	0	25	58	103
10	H	CF_3	trace	0	<10	343

the above observation that H_2 production is competitive with reduction of ketones. Additionally, electron-withdrawing substituents on alkyl part of ketones were also identified to prevent pinacol production, where only trace alcohol was perceived (subs. 10). Unsatisfied, the developed catalytic system is selective towards aromatic ketones (Table S2). Aliphatic ketones only deliver alcohol products with less than 10% yield. Heteroaromatic ketones, such as acetylpyridine and acetylfuran almost inactivate. Although unexpected limitations of this protocol displays, photocatalysis in the system has still demonstrated a particularly appealing strategy towards tackling the grand challenge of ketone conversion to useful chemicals.

3.2. Mechanism study

3.2.1. Radical clock experiment

To disclose the potential intermediates for pinacol coupling, the operation was carried out under O_2 atmosphere. Under the identical condition, only 5% yield of pinacol from acetophenone was obtained. Due to the radical removal feature of O_2, much lower transformation into pinacol clearly evidenced a radical intermediate was involved. However, this radical clock experiment is unable to distinguish the category of key radical during photocatalytic process. Therefore, an effective scavenger of carbon radicals, 4-tert-butylcatechol (TBC) was added to the reaction system. It is well known that the phenolic OH group on TBC can easily split to generate phenoxyl radical and hydrogen radical as the input energy is increased [7,23]. The hydrogen radical can efficiently capture carbon radical and intercept it for further transformation. As expected, in the appearance of 0.5 mmol of TBC, the outcome of the reaction was seriously interfered and no pinacol product was detected (Fig. S4), which implies a carbon radical is explicitly validated for the accomplishment of pinacol under the ambient condition.

Historically, Photo-irradiation assisted C-C bond formation was commonly proposed by collision and homo-dimerization of two ketyl radicals (Scheme 1) [24]. In recent years, a controversial finding comes from a reason that the concentration of active radical species is extremely low and the life-times are too short in solution [25]. Instead, alternative route to form the C-C bond can proceed via ketyl radical addition to the unsaturated C═O moiety of neighboring ketone (Scheme 1, right). The discrimination between the two possible interceptions of ketyl radical remains elusive until now. Therefore, a "potential cross coupling" reaction was designed to disclose the "historical mystery" for C-C bond formation. The equivalent acetophenone and benzaldehyde were applied for photocatalytic reaction under identical conditions. No

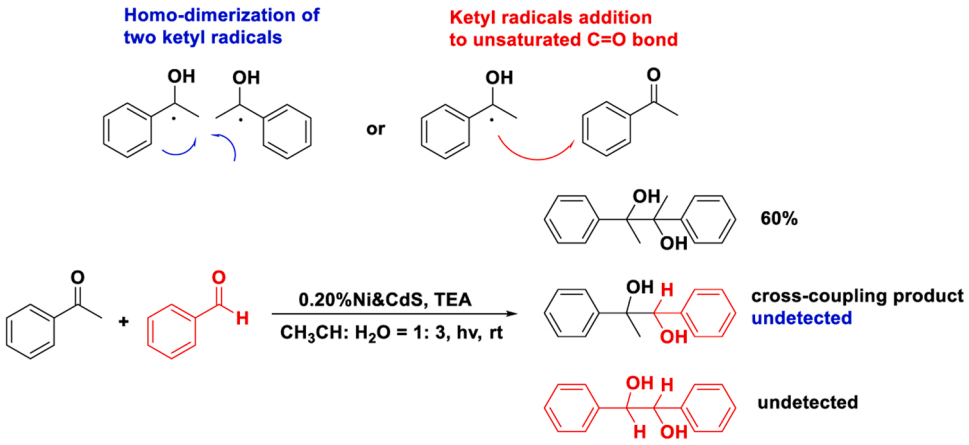

Scheme 1. The trial to determine the possibility of two representative C-C formation mechanism based on the cross-coupling test in the presence of acetophenone (1 mmol) and benzaldehyde (1 mmol) in a total 5 mL reaction system (H_2O: CH_3CN: TEA= 3: 1: 1) with 0.20% Ni&CdS (10 mg) under irradiation of 420 nm LED.

cross-coupling product and dimerization species from benzaldehyde were detected except for pinacol originated from acetophenone. Adjusting the ratio of acetophenone and benzaldehyde delivered the same results. Hence, it elucidates that ketyl radical generated from ketone is inactive to combine with C═O moiety on benzaldehyde. Alternatively, the coupling reaction between two C radicals is much faster and once the carbon radical is formed, the addition to C═O pendant is irreversibly suppressed. This result agrees well on the historical perspective that C-C bond coupling roots from homo-dimerization of two ketyl radical. Simultaneously, it is also manifested that distinct deterioration in reduction to 1-phenylethanol from acetophenone is attributed to fast coupling reaction rate of two C radical.

3.2.2. *Photo-excited electrons trapped function of Ni-doped CdS QDs on surface*

Read from photocatalytic result, it is distinctly announced that after doping Ni^{2+} into CdS, the reductive ability of photocatalyst for pinacol coupling is dramatically improved. To deeply probe the outstanding reduction behavior of 0.20% Ni&CdS QDs, the function of Ni dopants was carefully hashed over. Time-resolved flash photolysis on photocatalysts was initially inspected, which was applied to monitor the dynamic ET event on QDs surface. As shown in Fig. 3, both CdS and 0.20% Ni&CdS QDs display the similar profiles ranging from 375 nm to 550 nm with a broad bleaching centered at 432 nm under irradiation. Fits of lifetime at 432 nm displays a decay rate of the characteristic absorption, where biexponential curves yield a shorter lifetime of 41.8 ns and a

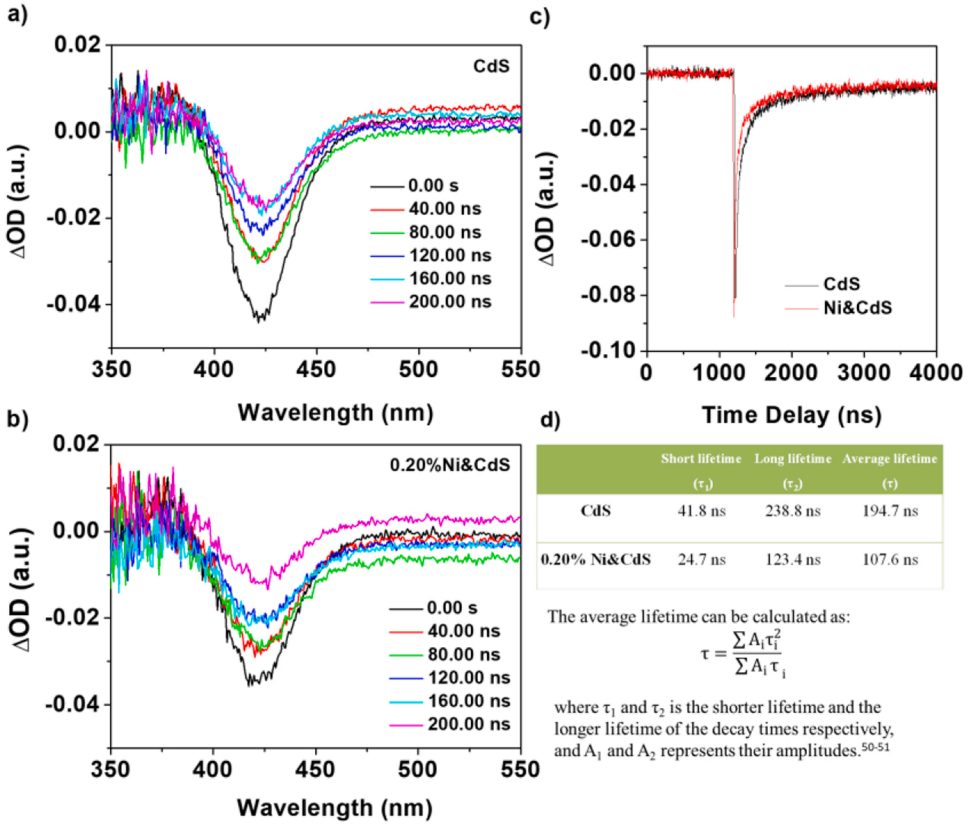

Fig. 3. The transit absorption of a) CdS and b) 0.20% Ni&CdS photocatalysts in the mixture of CH_3CN: H_2O (1:3) with irradiation using 355 nm laser respectively; c) the absorption decay at 423 nm of above systems; d) the short, long and average lifetime of each case respectively.

longer lifetime of 238.8 ns respectively in pristine CdS system. Based on literature, they represent the radiative recombination process of electrons and holes on band-edge and mid-gap respectively [26]. With Ni dopants, the excited-decay of QDs is accelerated with longer and shorter lifetime both shortened to 24.7 ns and 123.4 ns respectively.

Furthermore, the photoluminescence (PL) was associated to examine the charge behavior of QDs, which is often regulated through metal doping. PL intensity is usually dictated by the competition between the non-radiative and radiative relaxations on QDs surface [27]. During fluorescence excitation, photo-generated electron, which is promoted to the excited Conducted Band (CB), then undergoes a very fast non-radiative relaxation to the emissive state, following a radiative relaxation with holes in Valence Band (VB). Excitation at 380 nm resulted in typical band edge emission and trap emission at 440 and 561 nm respectively for pristine CdS QDs (Fig. S5) [28]. In the addition of Ni dopant, the trap emission was quenched, accompanied by the maximum red-shifted from 561 to 570 nm, which is attributed to the stronger influence exerted by the appearance of Ni dopants. In Ni dopants free system, photo-irradiation renders electrons are drawn by CB on CdS QDs, which will transfer to the surface and relax to surface defect states. Upon doping Ni^{2+}, the defects or traps on the nuclei surface can favor to introduce Ni dopant into CdS crystalline, and passivate the surface trap sites of QDs, which renders the photo-excited electrons would transfer to Ni dopant in sulfur vacancies and relax to shallow charge trap states. Accordingly, quenched PL associated with faster decay and shortened lifetime is typical feather assigned to ET on Ni&CdS

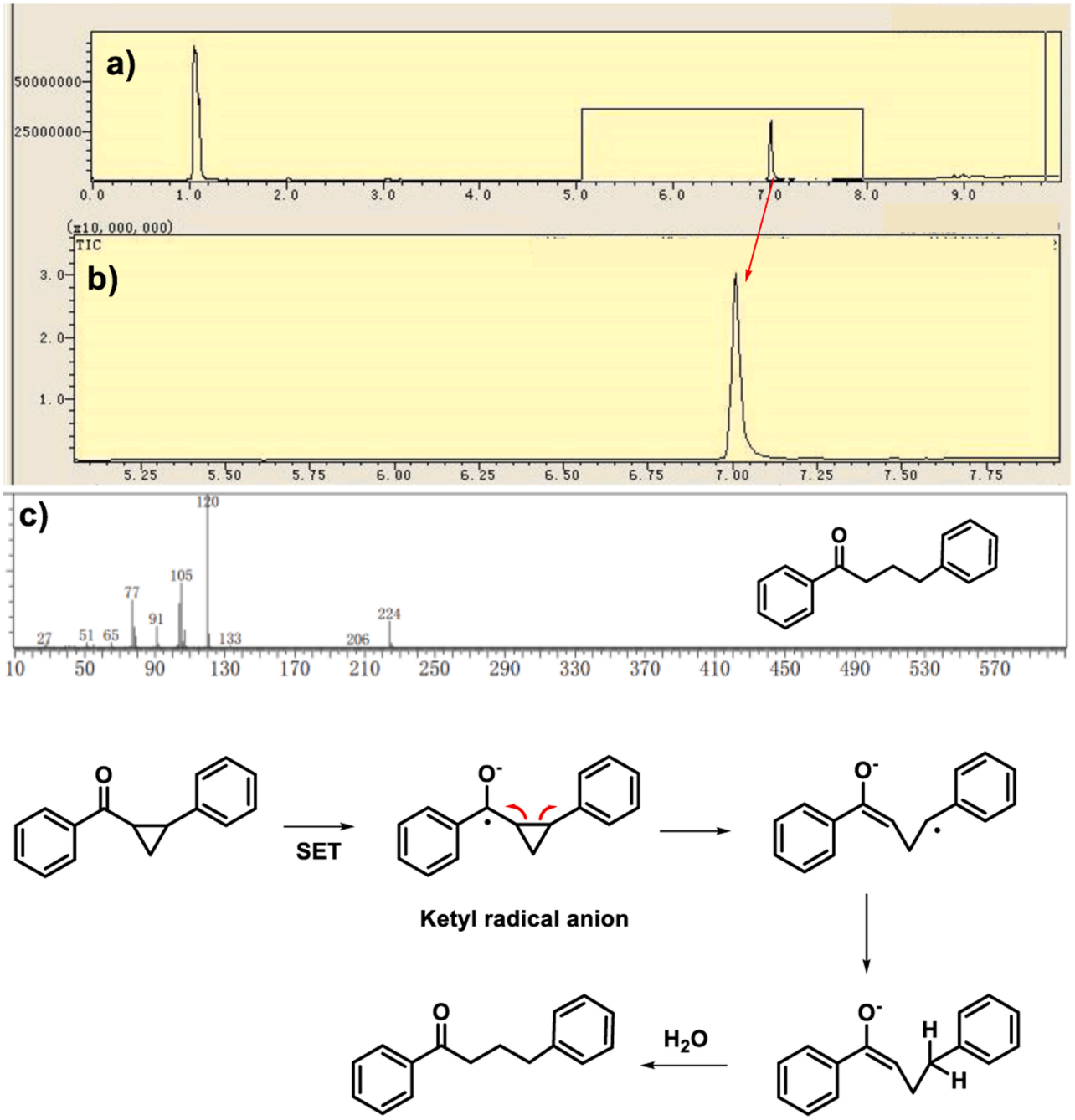

Fig. 4. The considered SET pathway for the reduction of phenyl (2-phenylcyclopropyl) methanone. a) The full GC-MS spectra of the product after photocatalytic phenyl (2-phenylcyclopropyl) methanone over 0.20% Ni&CdS QDs under the typical conditions; b) the peak assigned to the ring opening product in GC-MS; c) the MS spectra of the ring opening product in the system.

QDs surface [22]. In this regard, more electrons were trapped, rather than radiative recombination with holes, leading to the reduced recombination rate of photo-generated carriers and PL quenching [22]. Therefore, stemmed from both dynamic transit measurement and PL characterization in the system, it is reasonable to conclude that the addition of Ni dopants can enhance the electron trapping in sulfur vacancies so as to substantially promote charge separation, which is essential for further reduction of acetophenone.

3.2.3. SET distinguished experiments

Based on above analysis, the construction of C-C framework in pinacol undergoes a ketyl radical coupling. Taken account on a SET process responsible for the generation of carbon radical, the further strong evidence to the proposal lies on the use of phenyl (2-phenylcyclopropyl) methanone as a prevailing diagnostic probe [29]. It is accepted that SET can trigger cyclopropane ring opening with a rate constant in the range from 10^5 to 10^7 s^{-1}. That is different from the metal-hydride intermediates mechanism, in which the reduction of C═O moiety is dominant rather than cyclopropane ring opening. As depicted in Fig. 4, under the applied condition in our case, the reduction of phenyl (2-phenylcyclopropyl) methanone affords the ring-opening complex as the sole product in 80% yield. In this regard, it is that a SET process from photo-redox catalyst Ni&CdS to ketone not a metal-hydride intermediate to activate C═O pendant was involved for delivering the corresponding ketyl radical.

3.2.4. The reduction of acetophenone

EPR (Electron Paramagnetic Resonance) measurements of adducts were further exerted under the identical conditions to monitor the reduction of acetophenone. Control experiments were initiated. In the dark, no visible signal was detected. However, in the absence of acetophenone but under irradiation, typical signals ascribed to $^{\bullet}$OH radicals and $^{\bullet}$C radicals were detected in the mixture of TEA and photocatalysts with the help of 5,5-dimethyl-1-pyrroline-N-oxide (DMPO) (Fig. S6), but both were disappeared without TEA (Fig. S7). The percentage of two components was simulated by Simfonia software. DMPO-OH adduct was 84.5%, showing a quartet of peaks with an approximate intensity ratio of 1:2:2:1 ($\alpha_N = \alpha_H = 15.4$ G). DMPO-C radical adduct is 15.5%, holding a sextet signals with a ratio of 1:1:1:1:1:1 ($\alpha_N = 15.0$, $\alpha_H = 23.5$ G) [30]. The emergence of DMPO-OH adduct demonstrates that surface-adsorbed H_2O (OH^-) could be oxidized to $^{\bullet}$OH radicals by photo-generated holes, consistent with hydrogen production over Ni&CdS QDs surface [30c]. The DMPO-C radical adduct represents the formation of TEA$^{\bullet}$ radical, which is generated from the deprotonation of TEA$^{\bullet+}$ after TEA was oxidized by hole on Valence Band (VB) of Ni&CdS QDs [1c,2c,22b,30c,31].

The appearance of acetophenone gave rise to a much more complicated EPR spectrum shown in Fig. 5, implying a strong interplay between light, photocatalyst, substrate and TEA. By simulation, $^{\bullet}$OH radicals disappeared, which was totally replaced by three signals belonging to ketyl radical, saturated $^{\bullet}$C and $^{\bullet}$H radicals, with the percentage of 28.7%, 66.4% and 4.9% respectively. The DMPO-C radical adduct possesses the similar coupling constant with that in the absence of acetophenone, indicating the generation of degraded TEA. The emergence of $^{\bullet}$H radical may be generated from reduction of water, which is associated with alcohol generation or hydrogen production, but the percentage is quite low. Discerned from Fig. 5, sextet with an approximate intensity ratio of 1:1:1:1:1:1 ($\alpha_N = \alpha_H = 15.4$ G) featured the formation of ketyl radical adduct [1c,32]. This result correlates to SET mechanism, evidencing carbonyl group on acetophenone was reduced by outer sphere electron transfer [33]. Further comparison the percentage of each radical, it demonstrates that the amount of ketyl radical

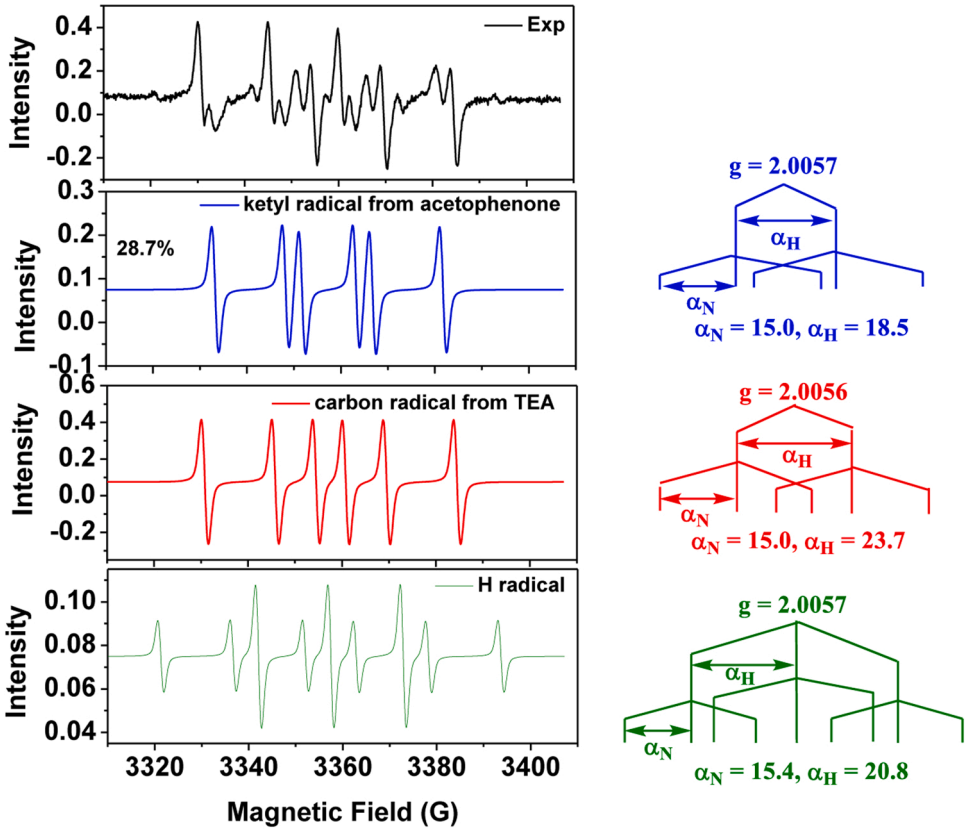

Fig. 5. Experimental (Exp) and simulated EPR spectra (blue, red and green curves) of adducts in the mixture of 0.20% Ni&CdS (2 mg mL^{-1}), acetophenone (0.4 M) and DMPO (0.12 M) with TEA (1 mL), CH_3CN (1 mL) and H_2O (3 mL), irradiated by LED (λ = 420 nm, the input optical power is 8.37 mW cm^{-2}) for 1.5 h under N_2 at room temperature.

is much higher than that of •H radical, implying ketyl radical is more easily coupled with each other rather than react with •H radical. Therefore, pinacol product dominated the whole conversion, in line with the observed superior selectivity for pinacol production to those for both hydrogen evolution and alcohol formation over Ni&CdS QDs activated system.

3.2.5. The function of TEA and PCET proposal for ketone activation

For traditional synthesis, photo-induced pinacol production usually demands high-energy ultraviolet light irradiation to activate C═O to yield excited ketones (triplets), which can easily abstract •H to form ketyl radicals [7]. However, in our case, photocatalysis was operated under visible-light irradiation, so it rule out the possibility that ketone was excited. Additional comment comes from the proposal that the generation of excited ketones via energy transfer process with the QD, but it can be also denied by the fact that no spectral overlap between the absorption of ketones at ground state and the emission of excited Ni&CdS QDs (Fig. S5 and S8).

As a sacrificial donor, TEA can feather as both electron donor and proton resource. Early in 2015, Rueping et al. reported the substrate-activated function of TEA in a photocatalytic conversion of ketone with Ru or Ir molecular photosensitizers [3a]. They proposed that the attractive interaction between in situ generated amino radical cation $TEA^{\bullet+}$ (after donating electron to excited photosensitizer) and C═O bond endows TEA with the advantages in serving as a functional activator for the umpolung of carbonyl derivatives into ketyl radical. Although the protocol is generally recognized, much stronger evidence has rarely been invoked to support $TEA^{\bullet+}$ mediated mechanism for substrate activation in organic synthesis until now. In order to probe the potential function of TEA and its impact on the overall photocatalytic C-C coupling of ketone, control experiments with different scavengers including triethanolamine (TEOA), *t*-butyl alcohol, Hantzsch Ester (HEH) as well as ascorbic acid (H_2A) was explored. The activities of the system were varied dramatically, even though the pH of reaction system has been adjusted to the same as TEA prior to the irradiation. Upon addition of TEOA, H_2A, HEH or *t*-butyl alcohol, H_2 was observed, but the pinacol formation was totally suppressed, whereas unclear by-product was produced instead. It is reported that in the presence of TEOA or H_2A, •H can be formed for liberating H_2 with CdS as photocatalyst [22b, 34]. Therefore, this result excludes the possibility that ketyl radical is generated from the attack of C═O bond by **•H** in the system in the appearance of TEA as sacrificial donor [35]. More distinctly, it implies that TEA can tailor the selectivity of photocatalysis in the presence of ketone and fascinate for the formation of ketyl radical.

Jointed density functional theory (DFT) calculation with experimental results, the role of TEA in photocatalytic reduction of ketone was further hashed over (Fig. 6). As a Lewis acid, $TEA^{\bullet+}$ can attractively interact with the weakly basic C═O group to form a two-center/three-electron intermediate [3a,36]. Alternatively, C-bound α-H can also fascinate to interact with C═O moiety for generation of intermediate **IM1** (shown in Fig. 6), which can readily engage in C═O activation in the forms of hydrogen bond. Based on calculation, the distance between α-H in $TEA^{\bullet+}$ and carbonyl O terminal is 2.67 Å and 2.57 Å respectively. Combined with the fact that **IM1** delivered a negative free energy as −1.1 kcal/mol, it indicates the interaction between $TEA^{\bullet+}$ and C═O group is more favorable to form **IM1**, although it is fragilely stable. In our reactions of interests, the proton sources could be water or TEA related species. However, the structures containing a ketyl radical and a hydroxy anion could not be optimized, which thereby precludes the possibility of water as proton sources. On the contrary, the $TEA^{\bullet+}$ radical cation is calculated to readily donate a proton. From the intermediate **IM2** in Fig. 6, a barrier-free proton transfer process from a N-adjacent CH site to C═O radical anion is located (**TS**, $\Delta G^{\ddagger}$ −1.8 kcal/mol), which further gives rise to **IM3** containing both a ketyl radical and a $TEA^{\bullet}$ radical (Fig. 6). The generated ketyl radical would undergo C-C radical coupling to yield pinacol product, which compelled **IM3** to liberate $TEA^{\bullet}$ for further degradation. $TEA^{\bullet+}$ was identified by addition of efficient capture for aminoalkyl radical adducts *N*-benzylidene-tert-butylamine *N*-oxide (PBN) (Fig. S9), remarked by an EPR signal with $\alpha_N = 14.9$ G [37]. Deprotonated $TEA^{\bullet}$ from $TEA^{\bullet+}$ and ketyl radical were successfully detected by EPR, as mentioned above. Iotope labeling experiments conducted with CH_3CN/D_2O mixture as solvent demonstrated no active hydrogen on terminal O was replaced by D atom in the deuterium pinacol fragment, which further supports the standpoint with TEA acting as the proton donor rather than water (Fig. S10). This observation is in agreement with the previous reports, although the occurrence of isotope exchange between $TEA^{\bullet+}$ and D_2O is ineluctable [8,38]. Together with the evidence gathered by GC-MS in which the signal belongs to the degraded TEA derivative (a coupled product from $TEA^{\bullet}$ radical) was successfully observed (Fig. S11) [39], it witnessed that a feasible PCET pathway was involved in the elementary activation step for ketyl radical generation. Such the process can be also expressed by DFT calculation, in which exothermic free energy to generate **IM3** is as large as −10.1 kcal/mol, manifesting that the whole reacting conversion favors to form ketyl and $TEA^{\bullet}$ radicals via PCET. More distinctly, the calculated reduction potential of PCET is 200 mV lower than that in direct ET process (Table S3). It means that more favorable driving forces are complemented by PCET with diminished activation barrier, allowing PCET to proceed more smoothly than either competing transfer pathway.

3.2.6. Proposed mechanism

Overall, a mechanism based on the above observation can be established (Scheme 2) [2e,40]. Under visible light irradiation, charge separation was initiated, where photo-induced electrons transfer from CB were localized in sulfur vacancies through the agency of Ni dopants. On the other hand, holes on VB reacted with TEA to generate amino radical cation $TEA^{\bullet+}$. Then the formed Lewis acidic species $TEA^{\bullet+}$ is associated to interact with weakly basic C═O bond and then isomerized in terms of hydrogen bond intermediates **IM1**. Owing to much lower energy barrier, it can fascinate PCET to produce the key ketyl radical. Alternatively, photo-generated carriers can be also trapped by H_2O molecules on Ni&CdS QDs surface to form •H radical. If the concentration of ketyl radical is high on semiconductor surface, radical

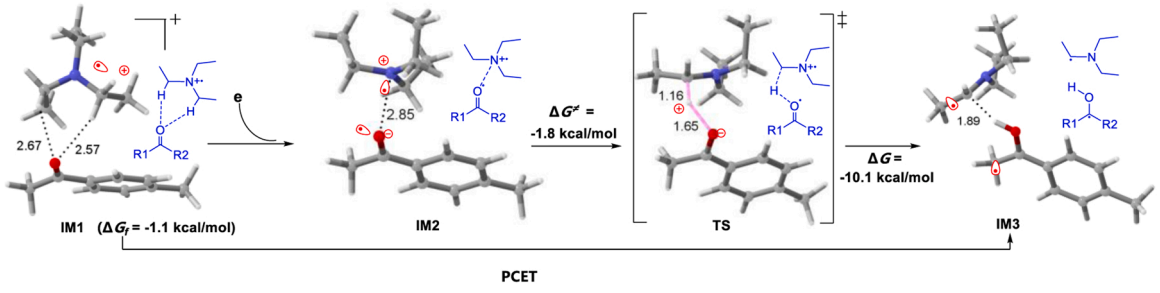

Fig. 6. The proposed imtermediates and transition state in PCET process of $TEA^{\bullet+}$ activated substrate system.

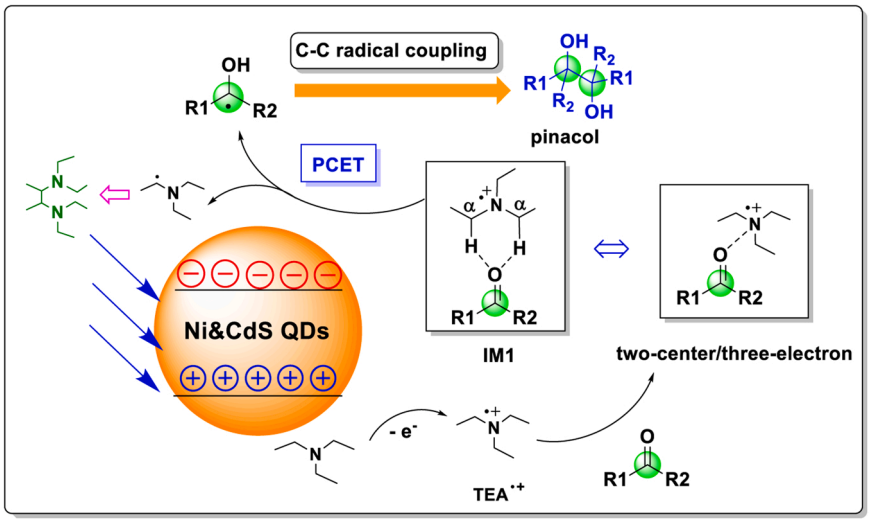

Scheme 2. The proposed mechanism for the generation of pinacol over Ni&CdS QDs.

homo-coupling will take place, and the desirable pinacol product will be formed. In contrast, if ketyl radical was captured by •H, alcohol product would boost as dominant product. Based on the experimental fact, the appearance of acetophenone could seriously suppress the reduction of water, therefore •H generation was difficult [22b]. As a result, it leads to a much lower concentration of •H, hence alcohol product was seriously inhibited. However, EPR measurement indicates the concentration of ketyl radical is much higher on QDs surface, which accordingly provides the dramatic enhancement in both higher selectivity and yield for pinacol generation.

4. Conclusion

In conclusion, we induced a robust photocatalytic process in which a visible-light driven aromatic ketone reduction into pinacol with desirable conversion and selectivity. Our ability to drive this reaction over a robust artificial photocatalysts Ni&CdS QDs revealed that Ni dopants in CdS lattice enable to effectively trap photo-excited electrons in sulfur vacancies. Subsequent dehydration of sacrificial reagent TEA was the key to activate ketone for the formation of the desired ketyl radical via PCET, which facilitates the homo-coupling and directs into pinacol as the major product. The overall mechanistic pathway accessed to generate pinacol products lays the foundation to understand the multiple roles of the sacrificial TEA, which is typically used as a sacrificial electron donor and explored to activate the substrates for mediating electron and proton. More importantly, this work puts forward a green and efficient way to produce valuable products from readily available feedstocks and heralds a new paradigm to perform reaction over the cheap light-harvesting semiconductors. Simultaneously, inspired by the research, a diversified interest can be explored to encompass synthesis of more complicated products, especially chiral complexes based on such simple and green pathway with further modifications. The related research is on-going now.

CRediT authorship contribution statement

Rong Hu: Visualization, Data curation, Formal analysis. **Wei-Hua Xie:** Visualization, Data curation, Formal analysis. **Hong-Yan Wang:** Visualization, Supervision, Formal analysis, Writing – review & editing, Funding acquisition. **Xin-Ai Guo:** EPR measurement and analysis. **Hua-Ming Sun:** EPR measurement and analysis. **Cheng-Bo Li:** Transit absorption measurement and analysis. **Xue-Peng Zhang:** DFT calculation, Writing – review & editing, Funding acquisition. **Rui Cao:** Visualization, Formal analysis, Review, Funding acquisition.

Declaration of Competing Interest

The authors declare that they have no known competing financial interests or personal relationships that could have appeared to influence the work reported in this paper.

Acknowledgements

National Natural Science Foundation of China (22072082, 21402113, 22003036), National Natural Science Foundation of Shaanxi Province (2019JQ-175), the Fundamental Research Funds for the Central Universities (GK202103026, GK202103033, GK202009068, GK201903041).

Appendix A. Supporting information

Supplementary data associated with this article can be found in the online version at doi:10.1016/j.apcatb.2021.120946.

REFERENCES

[1] (a) Z. Qiu, H.D.M. Pham, J. Li, C.C. Li, D.J. Castillo-Pazos, R.Z. Khaliullin, C.J. Li, Light-enabled metal-free pinacol coupling by hydrazine, Chem. Sci. 10 (2019) 10937–10943;
(b) T. Newhouse, P.S. Baran, R.W. Hoffmann, The economies of synthesis, Chem. Soc. Rev. 38 (2009) 3010–3021;
(c) L. Ren, M.-M. Yang, C.-H. Tung, L.-Z. Wu, H. Cong, Visible-light photocatalysis employing dye-sensitized semiconductor: selective aerobic oxidation of benzyl ethers, ACS Catal. 7 (2017) 8134–8138;
(d) T. Wirth, "New" reagents for the "Old" pinacol coupling reaction, Angew. Chem. Int. Ed. 35 (1996) 61–63;
(e) J. Xie, H. Jin, A.S.K. Hashmi, The recent achievements of redox-neutral radical C-C cross-coupling enabled by visible-light, Chem. Soc. Rev. 46 (2017) 5193–5203.
[2] (a) A. Bensari, J.-L. Renaud, O. Riant, Enantioselective pinacol coupling of aldehydes mediated and catalyzed by chiral titanium complexes, Org. Lett. 3 (2001) 3863–3865;
(b) A. Chatterjee, T.H. Bennur, N.N. Joshi, Truly catalytic and enantioselective pinacol coupling of aryl aldehydes mediated by chiral Ti(III) complexes, J. Org. Chem. 68 (2003) 5668–5671;
(c) Y. Hashimoto, U. Mizuno, H. Matsuoka, T. Miyahara, M. Takakura, M. Yoshimoto, K. Oshima, K. Utimoto, S. Matsubara, Structural studies of the low-valent titanium "solution": what goes on in the pinacol coupling reaction? J. Am. Chem. Soc. 123 (2001) 1503–1504;
(d) C.-J. Li, Organic reactions in aqueous media with a focus on carbon-carbon bond formations: a decade update, Chem. Rev. 105 (2005) 3095–3166;
(e) M. Paradas, A.G. Campaña, R.E. Estévez, L. Álvarez de Cienfuegos, T. Jiménez, R. Robles, J.M. Cuerva, J.E. Oltra, Unexpected Ti^{III}/Mn-promoted pinacol coupling of ketones, J. Org. Chem. 74 (2009) 3616–3619;
(f) N. Sotto, C. Cazorla, C. Villette, M. Billamboz, C. Len, Selective pinacol-coupling reaction using a continuous flow system, J. Org. Chem. 81 (2016) 11065–11071;

(g) J. Sun, Z. Dai, C. Li, X. Pan, C. Zhu, Enantioselective pinacol coupling reaction of aromatic aldehydes catalyzed by chiral vanadium complexes, J. Organomet. Chem. 694 (2009) 3219–3221.

[3] (a) M. Nakajima, E. Fava, S. Loescher, Z. Jiang, M. Rueping, Photoredox-catalyzed reductive coupling of aldehydes, ketones, and imines with visible light, Angew. Chem. Int. Ed. 54 (2015) 8828–8832;
(b) T. Shibata, A. Kabumoto, T. Shiragami, O. Ishitani, C. Pac, S. Yanagida, Novel visible-light-driven photocatalyst. Poly(p-phenylene)-catalyzed photoreductions of water, carbonyl compounds, and olefins, J. Phys. Chem. 94 (1990) 2068–2076.

[4] (a) K. Li, B. Peng, T. Peng, Recent advances in heterogeneous photocatalytic CO_2 conversion to solar fuels, ACS Catal. 6 (2016) 7485–7527;
(b) X. Liu, D. Sun, R. Yuan, X. Fu, Z. Li, Efficient visible-light-induced hydrogenation over composites of CdS and ruthenium carbonyl complexes, J. Catal. 304 (2013) 1–6;
(c) J. Xiao, X. Liu, L. Pan, C. Shi, X. Zhang, J.-J. Zou, Heterogeneous photocatalytic organic transformation reactions using conjugated polymers-based materials, ACS Catal. 10 (2020) 12256–12283;
(d) X. Zhou, N. Liu, P. Schmuki, Photocatalysis with TiO_2 nanotubes: "Colorful" reactivity and designing site-specific photocatalytic centers into TiO_2 nanotubes, ACS Catal. 7 (2017) 3210–3235;
(e) C. Huang, J. Qiao, R.-N. Ci, X.-Z. Wang, Y. Wang, J.-H. Wang, B. Chen, C.-H. Tung, L.-Z. Wu, Quantum dots enable direct alkylation and arylation of allylic C (sp^3)-H bonds with hydrogen evolution by solar energy, Chem 7 (2021) 1244–1257.

[5] (a) K.P. McClelland, E.A. Weiss, Selective photocatalytic oxidation of benzyl alcohol to benzaldehyde or C-C coupled products by visible-light-absorbing quantum dots, ACS Appl. Energy Mater. 2 (2018) 92–96;
(b) N. Luo, T. Hou, S. Liu, B. Zeng, J. Lu, J. Zhang, H. Li, F. Wang, Photocatalytic coproduction of deoxybenzoin and H_2 through tandem redox reactions, ACS Catal. 10 (2019) 762–769;
(c) Q. Guo, F. Liang, X.-B. Li, Y.-J. Gao, M.-Y. Huang, Y. Wang, S.-G. Xia, X.-Y. Gao, Q.-C. Gan, Z.-S. Lin, C.-H. Tung, L.-Z. Wu, Efficient and selective CO_2 reduction integrated with organic synthesis by solar energy, Chem 5 (2019) 2605–2616;
(d) T. Mitkina, C. Stanglmair, W. Setzer, M. Gruber, H. Kisch, B. Konig, Visible light mediated homo- and heterocoupling of benzyl alcohols and benzyl amines on polycrystalline cadmium sulfide, Org. Biomol. Chem. 10 (2012) 3556–3561;
(e) J.J. Zhong, W.P. To, Y. Liu, W. Lu, C.M. Che, Efficient acceptorless photo-dehydrogenation of alcohols and N-heterocycles with binuclear platinum(ii) diphosphite complexes, Chem. Sci. 10 (2019) 4883–4889.

[6] (a) K.T. Tarantino, P. Liu, R.R. Knowles, Catalytic ketyl-olefin cyclizations enabled by proton-coupled electron transfer, J. Am. Chem. Soc. 135 (2013) 10022–10025;
(b) L.J. Rono, H.G. Yayla, D.Y. Wang, M.F. Armstrong, R.R. Knowles, Enantioselective photoredox catalysis enabled by proton-coupled electron transfer: development of an asymmetric aza-pinacol cyclization, J. Am. Chem. Soc. 135 (2013) 17735–17738;
(c) E.C. Gentry, R.R. Knowles, Synthetic applications of proton-coupled electron transfer, Acc. Chem. Res. 49 (2016) 1546–1556.

[7] Y. Wang, P. Ren, X. Gu, X. Wen, Y. Wang, X. Guo, E.R. Waclawik, H. Zhu, Z. Zheng, Probing the mechanism of benzaldehyde reduction to chiral hydrobenzoin on the CNT surface under near-UV light irradiation, Green Chem. 18 (2016) 1482–1487.

[8] G. Han, X. Liu, Z. Cao, Y. Sun, Photocatalytic pinacol C-C coupling and jet fuel precursor production on $ZnIn_2S_4$ nanosheets, ACS Catal. 10 (2020) 9346–9355.

[9] A.Y. Li, A. Moores, Carbonyl reduction and biomass: a case study of sustainable catalysis, ACS Sustain. Chem. Eng. 7 (2019) 10182–10197.

[10] (a) Q.-Q. Bi, J.-W. Wang, J.-X. Lv, J. Wang, W. Zhang, T.-B. Lu, Selective photocatalytic CO_2 reduction in water by electrostatic assembly of CdS nanocrystals with a dinuclear cobalt catalyst, ACS Catal. 8 (2018) 11815–11821;
(b) K.M. Cho, K.H. Kim, K. Park, C. Kim, S. Kim, A. Al-Saggaf, I. Gereige, H.-T. Jung, Amine-functionalized graphene/CdS composite for photocatalytic reduction of CO_2, ACS Catal. 7 (2017) 7064–7069;
(c) K. Li, M. Han, R. Chen, S.L. Li, S.L. Xie, C. Mao, X. Bu, X.L. Cao, L.Z. Dong, P. Feng, Y.Q. Lan, Hexagonal@Cubic CdS core@shell nanorod photocatalyst for highly active production of H_2 with unprecedented stability, Adv. Mater. 28 (2016) 8906–8911;
(d) H.-Y. Wang, R. Hu, Y.-J. Lei, Z.-Y. Jia, G.-L. Hu, C.-B. Li, Q. Gu, Highly efficient and selective photocatalytic CO_2 reduction based on water-soluble CdS QDs modified by the mixed ligands in one pot, Catal. Sci. Technol. 10 (2020) 2821–2829;
(e) J. Yu, J. Jin, B. Cheng, M. Jaroniec, A noble metal-free reduced graphene oxide–CdS nanorod composite for the enhanced visible-light photocatalytic reduction of CO_2 to solar fuel, J. Mater. Chem. A 2 (2014) 3407–3416;
(f) M. Zhou, S. Wang, P. Yang, C. Huang, X. Wang, Boron carbon nitride semiconductors decorated with cds nanoparticles for photocatalytic reduction of CO_2, ACS Catal. 8 (2018) 4928–4936.

[11] (a) S. Berardi, S. Drouet, L. Francas, C. Gimbert-Surinach, M. Guttentag, C. Richmond, T. Stoll, A. Llobet, Molecular artificial photosynthesis, Chem. Soc. Rev. 43 (2014) 7501–7519;
(b) X.B. Li, C.H. Tung, L.Z. Wu, Quantum Dot assembly for light-driven multielectron redox reactions, such as hydrogen evolution and CO_2 reduction, Angew. Chem. Int. Ed. 58 (2019) 10804–10811;
(c) K. Wu, T. Lian, Quantum confined colloidal nanorod heterostructures for solar-to-fuel conversion, Chem. Soc. Rev. 45 (2016) 3781–3810.

[12] (a) D.J. Norris, A.L. Efros, S.C. Erwin, Doped nanocrystals, Science 319 (2008) 1776–1779;
(b) P.K. Santra, P.V. Kamat, Mn-doped quantum dot sensitized solar cells: a strategy to boost efficiency over 5%, J. Am. Chem. Soc. 134 (2012) 2508–2511;
(c) T. Simon, N. Bouchonville, M.J. Berr, A. Vaneski, A. Adrovic, D. Volbers, R. Wyrwich, M. Doblinger, A.S. Susha, A.L. Rogach, F. Jackel, J.K. Stolarczyk, J. Feldmann, Redox shuttle mechanism enhances photocatalytic H_2 generation on Ni-decorated CdS nanorods, Nat. Mater. 13 (2014) 1013–1018;
(d) J. Wang, T. Xia, L. Wang, X. Zheng, Z. Qi, C. Gao, J. Zhu, Z. Li, H. Xu, Y. Xiong, Enabling visible-light-driven selective CO_2 reduction by doping quantum dots: trapping electrons and suppressing H_2 evolution, Angew. Chem. Int. Ed. 57 (2018) 16447–16451.

[13] R. Gaussian, G. Trucks, H. Schlegel, G. Scuseria, M. Robb, J. Cheeseman, G. Scalmani, V. Barone, B. Mennucci, G. Petersson, H. Nakatsuji, M. Caricato, X. Li, H. Hratchian, A. Izmaylov, J. Bloino, G. Zheng, J. Sonnenberg, M. Hada, D. Fox, Gaussian, Gaussian, Inc., Wallingford, CT, Gaussian, Inc., Wallingford CT (2004).

[14] S. Grimme, S. Ehrlich, L. Goerigk, Effect of the damping function in dispersion corrected density functional theory, J. Comput. Chem. 32 (2011) 1456–1465.

[15] (a) A.D. Becke, Density-functional exchange-energy approximation with correct asymptotic behavior, Phys. Rev. A 38 (1988) 3098–3100;
(b) C. Lee, W. Yang, R.G. Parr, Development of the Colle-Salvetti correlation-energy formula into a functional of the electron density, Phys. Rev. B 37 (1988) 785–789;
(c) A.D. Becke, Density-functional thermochemistry. III. The role of exact exchange, J. Chem. Phys. 98 (1993) 5648–5652.

[16] (a) F. Weigend, R. Ahlrichs, Balanced basis sets of split valence, triple zeta valence and quadruple zeta valence quality for H to Rn: design and assessment of accuracy, Phys. Chem. Chem. Phys. 7 (2005) 3297–3305;
(b) F. Weigend, Accurate Coulomb-fitting basis sets for H to Rn, Phys. Chem. Chem. Phys. 8 (2006) 1057–1065.

[17] J. Tomasi, B. Mennucci, R. Cammi, Quantum mechanical continuum solvation models, Chem. Rev. 105 (2005) 2999–3094.

[18] A.V. Marenich, C.J. Cramer, D.G. Truhlar, Universal solvation model based on solute electron density and on a continuum model of the solvent defined by the bulk dielectric constant and atomic surface tensions, J. Phys. Chem. B 113 (2009) 6378–6396.

[19] (a) L.E. Roy, E. Jakubikova, M.G. Guthrie, E.R. Batista, Calculation of one-electron redox potentials revisited. is it possible to calculate accurate potentials with density functional methods? J. Phys. Chem. A 113 (2009) 6745–6750;
(b) C.P. Kelly, C.J. Cramer, D.G. Truhlar, Aqueous solvation free energies of ions and ion-water clusters based on an accurate value for the absolute aqueous solvation free energy of the proton, J. Phys. Chem. B 110 (2006) 16066–16081;
(c) H. Lei, A. Han, F. Li, M. Zhang, Y. Han, P. Du, W. Lai, R. Cao, Electrochemical, spectroscopic and theoretical studies of a simple bifunctional cobalt corrole catalyst for oxygen evolution and hydrogen production, Phys. Chem. Chem. Phys. 16 (2014) 1883–1893;
(d) Y. Han, Y. Wu, W. Lai, R. Cao, Electrocatalytic water oxidation by a water-soluble nickel porphyrin complex at neutral ph with low overpotential, Inorg. Chem. 54 (2015) 5604–5613;
(e) Y. Fu, L. Liu, H.-Z. Yu, Y.-M. Wang, Q.-X. Guo, Quantum-chemical predictions of absolute standard redox potentials of diverse organic molecules and free radicals in acetonitrile, J. Am. Chem. Soc. 127 (2005) 7227–7234.

[20] A.E. Reed, L.A. Curtiss, F. Weinhold, Intermolecular interactions from a natural bond orbital, donor-acceptor viewpoint, Chem. Rev. 88 (1988) 899–926.

[21] S.A. Snyder, S.B. Thomas, A.C. Mayer, S.P. Breazzano, Total syntheses of hopeanol and hopeahainol A empowered by a chiral Bronsted acid induced pinacol rearrangement, Angew. Chem. Int. Ed. 51 (2012) 4080–4084.

[22] (a) M. Luo, Y. Liu, J. Hu, H. Liu, J. Li, One-pot synthesis of CdS and Ni-doped CdS hollow spheres with enhanced photocatalytic activity and durability, ACS Appl. Mater. Interfaces 4 (2012) 1813–1821;
(b) J.J. Wang, Z.J. Li, X.B. Li, X.B. Fan, Q.Y. Meng, S. Yu, C.B. Li, J.X. Li, C. H. Tung, L.Z. Wu, Photocatalytic hydrogen evolution from glycerol and water over nickel-hybrid cadmium sulfide quantum dots under visible-light irradiation, ChemSusChem 7 (2014) 1468–1475;
(c) T. Hua, K. Daia, J. Zhang, S. Chen, Noble-metal-free Ni_2P modified step-scheme $SnNb_2O_6$/CdSdiethylenetriamine for photocatalytic hydrogen production under broadband light irradiation, Appl. Catal. B Environ. 269 (2021) 118844–118855;
(d) Y. Quan, G. Wang, Z. Jin, Tactfully assembled CuMOF/CdS S-scheme heterojunction for high-performance photocatalytic h2 evolution under visible light, ACS Appl. Energy Mater. 4 (2021) 8550–8562.

[23] (a) D.D. Li, R.M. Han, R. Liang, C.H. Chen, W. Lai, J.P. Zhang, L.H. Skibsted, Hydroxyl radical reaction with trans-resveratrol: initial carbon radical adduct formation followed by rearrangement to phenoxyl radical, J. Phys. Chem. B 116 (2012) 7154–7161;
(b) W.J. Runckel, L.A. Goldblatt, Inhibition of myrcene polymerization during storage, Ind. Eng. Chem. 38 (1946) 749–751.

[24] (a) S.G. Cohen, R.J. Baumgarten, Photoreduction of benzophenone by amines, alcohols, and hydrocarbons. Medium effects. Photochemical oxidative deamination, J. Am. Chem. Soc. 89 (1967) 3471–3475;
(b) S.G. Cohen, A. Parola, G.H. Parsons, Photoreduction by amines, Chem. Rev. 73 (1973) 141–161;
(c) J.N. Pitts, R.L. Letsinger, R.P. Taylor, J.M. Patterson, G. Recktenwald, R. B. Martin, Photochemical reactions of benzophenone in alcohols1, J. Am. Chem. Soc. 81 (1959) 1068–1077;
(d) Y. Shen, Y. Gu, R. Martin, sp3C-H arylation and alkylation enabled by the synergy of triplet excited ketones and nickel catalysts, J. Am. Chem. Soc. 140 (2018) 12200–12209.

[25] (a) H. Fischer, The persistent radical effect: a principle for selective radical reactions and living radical polymerizations, Chem. Rev. 101 (2001) 3581–3610;
(b) D. Leifert, A. Studer, The Persistent Radical Effect in Organic Synthesis, Angew. Chem. Int. Ed. 59 (2020) 74–108.

[26] (a) K.E. Knowles, E.A. McArthur, E.A. Weiss, A. Multi-Timescale, Map of radiative and nonradiative decay pathways for excitons in CdSe quantum dots, ACS Nano 5 (2011) 2026–2035;
(b) I. Lignos, R.M. Maceiczyk, M.V. Kovalenko, S. Stavrakis, Tracking the fluorescence lifetimes of cesium lead halide perovskite nanocrystals during their synthesis using a fully automated optofluidic platform, Chem. Mater. 32 (2020) 27–37.

[27] (a) Y. Ben-Shahar, F. Scotognella, N. Waiskopf, I. Kriegel, S. Dal Conte, G. Cerullo, U. Banin, Effect of surface coating on the photocatalytic function of hybrid CdS-Au nanorods, Small 11 (2015) 462–471;
(b) E. Zillner, S. Fengler, P. Niyamakom, F. Rauscher, K. Köhler, T. Dittrich, Role of ligand exchange at CdSe quantum dot layers for charge separation, J. Phys. Chem. C 116 (2012) 16747–16754.

[28] J. Jasieniak, P. Mulvaney, From Cd-Rich to Se-Rich - the manipulation of CdSe nanocrystal surface stoichiometry, J. Am. Chem. Soc. 129 (2007) 2841–2848.

[29] A. Call, C. Casadevall, F. Acuna-Pares, A. Casitas, J. Lloret-Fillol, Dual cobalt-copper light-driven catalytic reduction of aldehydes and aromatic ketones in aqueous media, Chem. Sci. 8 (2017) 4739–4749.

[30] (a) H. Belhadj, S. Melchers, P.K.J. Robertson, D.W. Bahnemann, Pathways of the photocatalytic reaction of acetate in H_2O and D_2O: a combined EPR and ATR-FTIR study, J. Catal. 344 (2016) 831–840;
(b) G. Feng, P. Cheng, W. Yan, M. Boronat, X. Li, J.-H. Su, J. Wang, Y. Li, A. Corma, R. Xu, J. Yu, Accelerated crystallization of zeolites via hydroxyl free radicals, Science 351 (2016) 1188–1191;
(c) Z.J. Li, J.J. Wang, X.B. Li, X.B. Fan, Q.Y. Meng, K. Feng, B. Chen, C.H. Tung, L. Z. Wu, An exceptional artificial photocatalyst, Nih -CdSe/CdS core/shell hybrid, made in situ from CdSe quantum dots and nickel salts for efficient hydrogen evolution, Adv. Mater. 25 (2013) 6613–6618.

[31] V.N. Belevskii, S.I. Belopushkin, K.B. Nuzhdin, ESR study of the mechanism of radical formation during liquid-and solid-phase radiolyses of ethylamines, High. Energy Chem. 41 (2007) 10–19.

[32] (a) Q. Guo, S.Y. Qian, R.P. Mason, Separation and identification of DMPO adducts of oxygen-centered radicals formed from organic hydroperoxides by HPLC-ESR, ESI-MS and MS/MS, J. Am. Soc. Mass Spectrom. 14 (2003) 862–871;
(b) F.A. Villamena, E.J. Locigno, A. Rockenbauer, C.M. Hadad, J.L. Zweier, Theoretical and experimental studies of the spin trapping of inorganic radicals by 5,5-dimethyl-1-pyrroline N-oxide (DMPO). 1. Carbon Dioxide radical anion, J. Phys. Chem. A 110 (2006) 13253–13258;
(c) S. Xie, Z. Shen, J. Deng, P. Guo, Q. Zhang, H. Zhang, C. Ma, Z. Jiang, J. Cheng, D. Deng, Y. Wang, Visible light-driven C-H activation and C-C coupling of methanol into ethylene glycol, Nat. Commun. 9 (2018) 1181–1188.

[33] (a) S. Chen, C. Yin, T. Jiang, M. Gao, Y. Chen, D.-Y. Wu, Y. Yu, A. Zhang, Y. Fang, Triethylamine as a complexing reagent for highly efficient naked-eyes copper ions sensing - a new catalytic pathway for ultrasensitive detection, Sens. Actuators B Chem. 305 (2020) 127373–127380;
(b) W. Miao, J.-P. Choi, A.J. Bard, Electrogenerated chemiluminescence 69: the tris(2,2′-bipyridine)ruthenium(II), $(Ru(bpy)_3^{2+})$/Tri-n-propylamine (TPrA) system revisiteda new route involving $TPrA^{\bullet+}$ cation radicals, J. Am. Chem. Soc. 124 (2002) 14478–14485.

[34] C. Liu, Y. Yang, W. Li, J. Li, Y. Li, Q. Shi, Q. Chen, Highly efficient photoelectrochemical hydrogen generation using $Zn_xBi_2S_{3+x}$ sensitized platelike WO_3 photoelectrodes, ACS Appl. Mater. Interfaces 7 (2015) 10763–10770.

[35] J.P. Moerdyk, D. Schilter, C.W. Bielawski, N,N′-diamidocarbenes: isolable divalent carbons with bona fide carbene reactivity, Acc. Chem. Res. 49 (2016) 1458–1468.

[36] Q. Xia, J. Dong, H. Song, Q. Wang, Visible-light photocatalysis of the ketyl radical coupling reaction, Chem. Eur. J. 25 (2019) 2949–2961.

[37] W. Sheng, J.L. Shi, H. Hao, X. Li, X. Lang, Selective aerobic oxidation of sulfides by cooperative polyimide-titanium dioxide photocatalysis and triethylamine catalysis, J. Colloid Interface Sci. 565 (2020) 614–622.

[38] T.U. Connell, C.L. Fraser, M.L. Czyz, Z.M. Smith, D.J. Hayne, E.H. Doeven, J. Agugiaro, D.J.D. Wilson, J.L. Adcock, A.D. Scully, D.E. Gomez, N.W. Barnett, A. Polyzos, P.S. Francis, The tandem photoredox catalysis mechanism of $[Ir(ppy)_2(dtb\text{-}bpy)]^+$ enabling access to energy demanding organic substrates, J. Am. Chem. Soc. 141 (2019) 17646–17658.

[39] M. Berton, R. Mello, R. Acerete, M.E. González Núñez, Photolysis of tertiary amines in the presence of CO_2: the paths to formic acid, α-Amino acids, and 1,2-diamines, J. Org. Chem. 83 (2018) 96–103.

[40] (a) H.C. Aspinall, N. Greeves, C. Valla, Samarium diiodide-catalyzed diastereoselective pinacol couplings, Org. Lett. 7 (2005) 1919–1922;
(b) J.V. Kingston, O.V. Ozerov, S. Parkin, C.P. Brock, F.T. Ladipo, Mechanistic Insight into fragmentation reactions of titanapinacolate complexes, J. Am. Chem. Soc. 124 (2002) 12217–12224;
(c) J.E. McMurry, W. Choy, The mechanism of the thermal isomerization of 1,2-diolates. Is the pinacol coupling reaction reversible? J. Org. Chem. 43 (1978) 1800–1803.